NANO LETTERS

pubs.acs.org/NanoLett

Letter

Cavity-Enhanced Circular Dichroism in a van der Waals Antiferromagnet

Shuliang Ren,[†] Simin Pang,[†] Shan Guan, Yu-Jia Sun, Tian-Yu Zhang, Nai Jiang, Jiaqi Guo, Houzhi Zheng, Jun-Wei Luo, Ping-Heng Tan, Chao Shen,* and Jun Zhang*

Cite This: *Nano Lett.* 2025, 25, 2709−2715

Read Online

ACCESS | Metrics & More | Article Recommendations | Supporting Information

ABSTRACT: Broken symmetry plays a pivotal role in determining the macroscopic electrical, optical, magnetic, and topological properties of materials. Circular dichroism (CD) has been widely employed to probe broken symmetry in various systems, from small molecules to bulk crystals, but designing CD responses on demand remains a challenge, especially for antiferromagnetic materials. Here we develop a cavity-enhanced CD technique to sensitively probe the magnetic order and broken symmetry in the van der Waals antiferromagnet $FePS_3$. By introducing interfacial inversion asymmetry in cavity-coupled $FePS_3$ crystals, we demonstrate that the induced CD is strongly coupled with the zigzag antiferromagnetic order of $FePS_3$ and can be tuned both spectrally and in magnitude by varying the cavity length ($FePS_3$ thickness). Our findings open new avenues for using cavity-modulated CD as a sensitive diagnostic probe to detect weak broken symmetries, particularly at hidden interfaces, and in systems exhibiting hidden spin polarization or strong correlations.

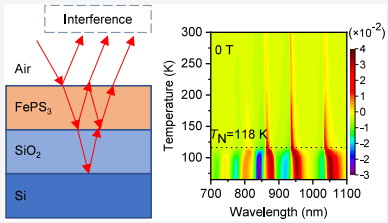

KEYWORDS: *circular dichroism, cavity, van der Waals antiferromagnet, $FePS_3$*

The investigation of magnetic order and broken symmetry in two-dimensional (2D) magnetic materials has attracted widespread attention[1−3] due to its importance for the development of 2D magnetic-related devices, such as magnetic storage and on-chip quantum communication.[4−7] Therefore, it is imperative to directly probe and manipulate the magnetic order and broken symmetry in 2D magnets. Techniques like natural circular dichroism (NCD) and magnetic circular dichroism (MCD) spectroscopy, which measure the difference in reflected or transmitted light intensity between left and right circularly polarized (LCP and RCP) light,[8−11] are sensitive probes for broken symmetry. NCD requires broken inversion symmetry, while MCD emerges in magnetic materials with broken time-reversal symmetry, typically induced by an external magnetic field oriented along the direction of light propagation.[12] Notably, the behavior of NCD and MCD is different for light propagation reversal: NCD accumulates in a cavity, enhancing the signal, while the MCD accumulated in the forward direction is compensated by backward propagation, making them less sensitive in cavities. The cavity-enhanced effect for NCD and MCD is different from the case for optical rotation and Faraday rotation,[13] as schematically shown in Figure S1.

In 2D materials, typical magnetic orders include ferromagnetism and antiferromagnetism.[14] Compared to ferromagnetic materials, 2D antiferromagnetic (AFM) materials, such as $FePS_3$, offer higher response frequency and no stray fields, making them promising for the next generation of AFM spintronics devices.[15−17] $FePS_3$, an Ising-type van der Waals AFM, can be easily exfoliated to atomic thickness, retaining long-range magnetic order even at the monolayer limit, providing a unique platform for conducting fundamental studies related to 2D AFM properties.[18,19] Previous studies have demonstrated several attractive phenomena in $FePS_3$, including a giant out-of-plane magnetic anisotropy,[20] near-unity linear dichroism (LD),[21] giant surface second-harmonic generation (SHG) coupled to nematic orders,[22] divergence behavior of the demagnetization time near the magnetic phase transition investigated by magnetic linear birefringence (MLB) and optical pump-probe spectroscopy,[23] and magnon-phonon coupling studied by Raman spectroscopy.[24] Bulk $FePS_3$ has a monoclinic structure (space group $C2/m$), which is inversion symmetric, with a band gap of approximately 1.5 eV.[25] As shown in Figure 1a, iron (Fe) atoms are octahedrally coordinated by six sulfur (S) atoms at the vertices and form a honeycomb lattice in the *ab* plane. A pair of phosphorus (P) atoms is located at the center of each hexagon. The magnetic properties of $FePS_3$ are determined by the Fe *d*-electron. Below the Néel temperature (T_N), $FePS_3$ exhibits zigzag AFM order.[18] In the hexagonal honeycomb plane composed of Fe atoms, nearby zigzag chains have opposite spin orientations,

Received: November 13, 2024
Revised: January 27, 2025
Accepted: January 31, 2025
Published: February 6, 2025

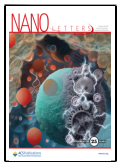

https://doi.org/10.1021/acs.nanolett.4c05724
Nano Lett. 2025, 25, 2709−2715

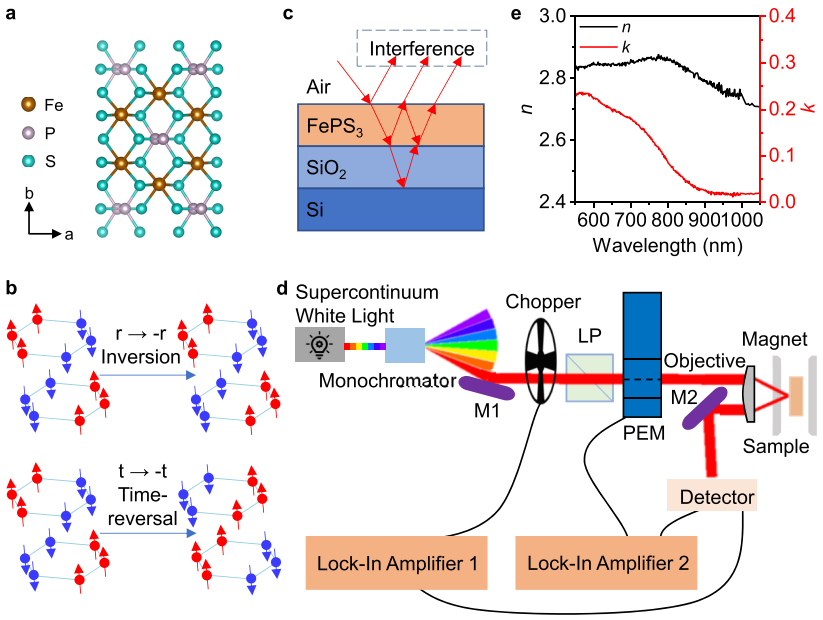

Figure 1. Structure, magnetic, and optical properties of $FePS_3$, together with the schematic optical interference and experimental setup for CD measurements. (a) Top view of the atomic lattice of the $FePS_3$ crystal. Brown, purple, and mint green spheres represent Fe, P, and S atoms, respectively. (b) Symmetry of the spin structure on the honeycomb lattice of Fe^{2+} at 0 T. Red and blue arrows represent spin up and spin down, respectively. The zigzag AFM order ($T < T_N$) in $FePS_3$ preserves the inversion symmetry (leading to a vanishing NCD) while breaking the time-reversal symmetry. However, the combination of the half-unit cell translational operation with the time-reversal operation is a good symmetry, resulting in a zero MCD. (c) Schematic of multiple reflection and optical interference in the cavity-enhanced CD spectra measurements. (d) Schematic of the experimental setup for CD measurements. The M, LP, and PEM represent mirror, linear polarizer, and photoelastic modulator, respectively. (e) Optical constants of bulk $FePS_3$ measured with an ellipsometer at room temperature.

i.e., spin up and spin down perpendicular to the honeycomb plane, respectively, as shown by the red and blue arrows in Figure 1b. The adjacent planes are coupled antiferromagnetically. In the paramagnetic (PM) state ($T > T_N$), $FePS_3$ is structurally centrosymmetric. Below T_N, $FePS_3$ undergoes a magnetic phase transition to the AFM state, accompanied by a simultaneous structural phase transition. Across the phase transition, the crystal structure remains monoclinic, but the monoclinic angle experiences a subtle and abrupt change.[26,27] Figure 1b shows that the zigzag AFM order preserves the inversion symmetry. Therefore, for $FePS_3$ in both the PM and AFM states, the NCD vanishes. Additionally, despite the broken time-reversal symmetry due to the zigzag AFM,[28] the combined half-unit cell translation and time-reversal symmetry preserves the band Kramers degeneracy, resulting in zero MCD. This absence of NCD and MCD in fully compensated collinear AFM $FePS_3$ prevents them from being appropriate probes. Inducing a nonzero CD in the $FePS_3$ system and enhancing it is essential for detecting antiferromagnetism and advancing applications based on antiferromagnets.

In this report, we studied the magnetic order and broken symmetry of $FePS_3$ using cavity-enhanced CD spectroscopy. By constructing an asymmetric interface between $FePS_3$ and the substrate, we induced a small, nonzero NCD, which is accompanied by an interfacial spin-orbit magnetic field (B_0). This induced NCD is highly sensitive to both the interfacial structure and spin asymmetry and can be further enhanced through the interference effect. By adjusting the cavity length ($FePS_3$ thickness), the strength of NCD can be modulated. Notably, below T_N, the increased asymmetry in both spin and structure at the interface results in a significant enhancement of the CD signal, serving as a clear indicator of magnetic phase transitions and spin ordering. These findings present cavity-enhanced CD as a promising tool to explore antiferromagnetism and broken symmetries in materials where conventional probes struggle due to the absence of net magnetization.

When the material has low light absorption, the interference effect becomes prominent at a certain thickness. Figure 1c shows a schematic of multiple reflection and optical interference in a multilayer structure consisting of air, $FePS_3$ flake, SiO_2, and Si substrate, forming an optical cavity. This cavity enhances the CD by attenuating the reflected light due to the interference effect.[29] Since the samples were exfoliated on opaque substrates, we used the reflection setup rather than transmission. Reflectance CD measurements were conducted using a polarization modulation technique in our home-built microscopic system, as schematically shown in Figure 1d (detailed in Section 3 of the Supporting Information). Figure 1e shows the optical constants n and k of the bulk $FePS_3$ measured with an ellipsometer at room temperature. Mathematically, CD is defined as

$$\mathrm{CD} = \frac{R_+(E) - R_-(E)}{[R_+(E) + R_-(E)]/2} \propto \frac{1}{R}\frac{\mathrm{d}R(E)}{\mathrm{d}E}\Delta n \tag{1}$$

where R_+ (R_-) is the reflectance of LCP (RCP) light, $R = (R_+ + R_-)/2$ is the average reflectance without polarization, and Δn is the refractive index difference between LCP and RCP lights.[30−32] More details about the derivation of eq 1 can be found in Section 5 of the Supporting Information. The CD spectrum can be approximately the first-order differential of the modulated reflectance spectrum. An obvious CD appears at the minimum of the reflectance spectrum, which is proportional to Δn. The cavity-enhanced effect enables the detection of small Δn.

https://doi.org/10.1021/acs.nanolett.4c05724
Nano Lett. 2025, 25, 2709−2715

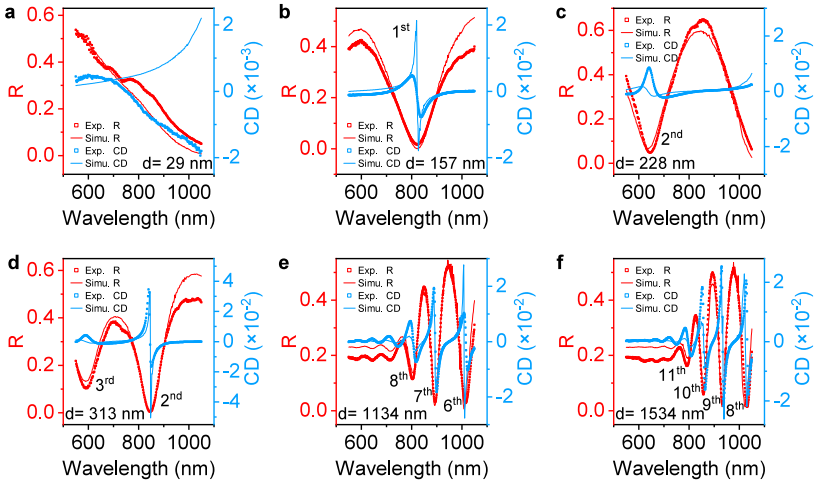

Figure 2. Experimental reflectance (red) and CD (blue) spectra of $FePS_3$ with different thicknesses on 90 nm SiO_2/Si substrate at −3 T and 300 K, together with the simulated curves: (a) 29, (b) 157, (c) 228, (d) 313, (e) 1134, and (f) 1534 nm. Different CD resonances are marked with their order number (p).

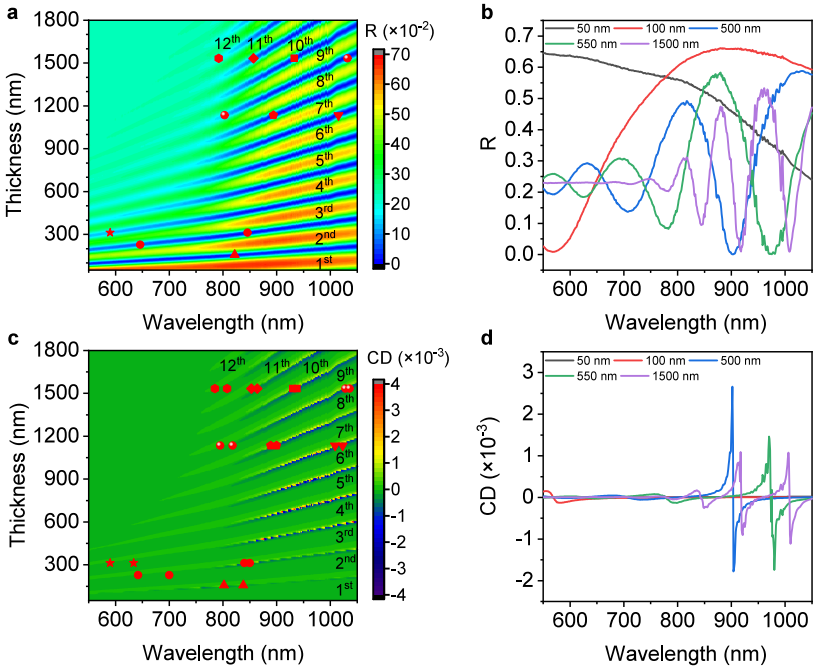

Figure 3. Simulated reflectance and CD spectra of $FePS_3$ on 90 nm SiO_2/Si substrate. (a) Reflectance and (c) corresponding CD intensity contour plot as a function of $FePS_3$ thickness, from 50 to 1800 nm at 10 nm intervals. The CD spectra were calculated from the reflectance spectra according to eq 1 with $\Delta n \approx 2.9548 \times 10^{-4}$. The red symbols in (a) and (c) represent the experimentally measured minimum reflectance and CD resonances with different orders extracted from Figure 2. (b) Reflectance and (d) CD spectra with several typical thicknesses (50, 100, 500, 550, and 1500 nm) extracted from (a) and (c), respectively.

$FePS_3$ with a specific thickness (d) can form an internal cavity, enhancing light-matter interaction and, thus, the CD. The cavity modes occur at wavelengths (λ) that satisfy $d = p\frac{\lambda}{2n_{\text{eff}}}$, where p represents the cavity mode order and n_{eff} denotes the effective refractive index of the stacked $FePS_3$/SiO_2/Si.[21] To demonstrate the cavity-enhanced CD effect, reflectance (red) and CD (blue) spectra were measured on $FePS_3$ with six distinct thicknesses (d) exfoliated on 90 nm SiO_2/Si substrate under −3 T and 300 K (symbols in Figure 2). As shown in Figure 2a, the 29 nm thick sample is unable to support cavity modes in the detection wavelength range, and no CD signal is observed. As the thickness increases, interference effects become more pronounced, with more characteristic signals in the reflectance spectra. The minimum reflectance corresponds to different orders of the cavity mode resonances, marked by their respective order numbers (p). The CD extremum, appearing on both sides of the corresponding minimum reflectance, also intensifies with increasing thickness and shifts toward longer wavelengths, indicating the interference effect's role in enhancing CD (Figure 2b–f). The simulated spectra were denoted by the solid lines in Figure 2. To match the experimental results, the Δn in eq 1 was estimated as 2.9548×10^{-4} for all wavelengths in our calculations, though it should be wavelength-dependent. As shown in Figure 2, the experimental reflectance and CD

https://doi.org/10.1021/acs.nanolett.4c05724
Nano Lett. 2025, 25, 2709−2715

spectra (symbols) mostly agree well with the simulated results (solid lines), particularly for thicker samples. However, a minor discrepancy exists between the experimental and simulated CD spectra for wavelengths below 827 nm (above the bandgap of 1.5 eV). In the CD spectrum calculations, we assumed that the CD primarily arises from the different responses of the real part of the complex refractive index (n) to the two circularly polarized lights, ignoring the effect of the weak imaginary part (k), which is valid when $n \gg k$, i.e., for wavelengths above 827 nm. Therefore, k and Δk cause deviations of the simulated results from the experimental spectra. Although the absolute values of the simulated reflectance and CD are less meaningful, our simulated results can still reproduce the shape characteristics of the experimental reflectance and CD spectra, and the intensity discrepancy would not affect our main conclusion.

To better understand the cavity-enhanced CD of the stacked $FePS_3/SiO_2/Si$, we calculated the reflectance and CD spectra for $FePS_3$ thicknesses from 50 to 1800 nm at 10 nm intervals. The calculated reflectance and CD intensity contour plots are shown in Figure 3a and c, respectively. The linearly dispersive branches of the resonances from bottom to top correspond to the first to 12th order cavity modes. The experimentally measured resonance positions of reflectance and CD extracted from Figure 2 are indicated by red symbols. For cavity modes of the same order, the CD signals are enhanced as the $FePS_3$ thickness increases due to more pronounced interference effects. Figure 3b and d display the reflectance and CD spectra for several typical thicknesses extracted from Figure 3a and c, respectively, intuitively displaying multiple orders of resonances. Notably, as shown in Figure 3c, $FePS_3$, with a thickness of less than 100 nm, exhibits no obvious CD as it is too thin to induce an interference effect and form an internal cavity for the photons within the detection wavelength region. Considering thin samples, we proposed that constructing an external cavity would also enhance the CD. We exfoliated an 80 nm $FePS_3$ on a distributed Bragg reflector (DBR) with a thickness of about 3 μm (Figure S2a). The CD is significantly enhanced here (Figure S2c), compared to the case on the 90 nm SiO_2/Si substrate, where neither the internal nor external cavities are formed. Similarly, increasing the SiO_2/Si substrate thickness would also support an external cavity. Our results demonstrate that forming the internal or external cavity is an efficient method to enhance the CD in both thick and thin samples. The resonance magnitude and spectral position of the CD can be tuned simply by altering the thickness (cavity length) of the $FePS_3$ or substrate.

At room temperature, $FePS_3$ is in the PM state, maintaining both inversion and time-reversal symmetry. Applying an external magnetic field would break the time-reversal symmetry, causing a nonzero MCD. The degree of broken time-reversal symmetry is proportional to the strength of the MCD. Since the thick sample possesses a more significant cavity-enhanced effect and thus a more apparent MCD, we investigated the magnetic field-dependent CD spectra at 300 K using the 1500 nm thick $FePS_3$ (S1 sample). The CD spectra show five interference characteristic wavelengths (around 1027, 930, 852, 784, and 721 nm), corresponding to the eighth to 12th order cavity modes (Figure 4a). Specifically, by constructing an asymmetric interface ($FePS_3/SiO_2/Si$ substrate) that breaks the interfacial inversion symmetry, we successfully generated and detected the NCD at 0 T (green curve in Figure 4a), which should vanish in centrosymmetric PM $FePS_3$. First, we can rule out that the finite CD at 0 T is

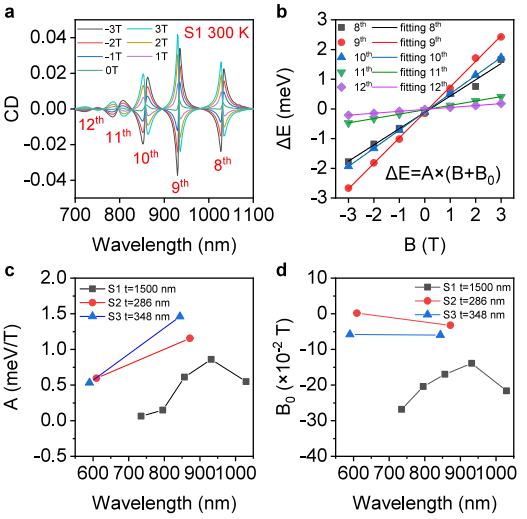

Figure 4. Magnetic field dependence of cavity-enhanced CD spectra of $FePS_3$ at 300 K. (a) Magnetic field-dependent CD spectra of S1 flake (1500 nm). Different CD resonances are marked with their order number (p). (b) Magnetic field-dependent energy splitting (ΔE) at specific wavelengths, extracted from (a). The symbols represent the experimental results, and the lines are the corresponding linear fitting results using the formula $\Delta E = A \times (B + B_0)$. Linear fitting parameters (c) A and (d) B_0 for three samples of different thicknesses.

attributed to the intrinsic ferromagnetism of $FePS_3$. As shown in Figure S3, the CD of the S1 sample measured from +0 T (down from the positive field) and −0 T (up from the negative field) was almost the same, indicating no hysteresis and $FePS_3$ is PM with no net magnetization at room temperature. The NCD exactly originates from the broken inversion symmetry at the $FePS_3/SiO_2$ interface, which would also introduce an interfacial spin-orbit magnetic field[33,34] (B_0). Besides the $FePS_3$/90 nm SiO_2/Si, the DBR substrate formed by periodic arrangements of SiO_2 and Ta_2O_5 also exhibits weak CD at 0 T, owing to its interfacial structural inversion asymmetry (Figure S2b).

Under a certain magnetic field, the electron energy levels of different spins in the sample split, which can be detected using the MCD. The energy splitting (ΔE) can be deduced from the MCD peak at energy E_1 and valley at E_2, that is $\Delta E = -\sqrt{e}\, w \frac{\Delta R_{\text{MCD-peak}} - \Delta R_{\text{MCD-valley}}}{2R_0}$, where $2w = |E_1 - E_2|$ and R_0 is the reflectance at energy $E_0 = (E_1 + E_2)/2$.[30] As shown in Figure 4b, the ΔE of five resonant cavity modes extracted from Figure 4a depends linearly on the external magnetic field B, which can be well fitted by $\Delta E = A \times (B + B_0)$, where A is the slope of the linear fit and B_0 represents the nonzero interfacial spin-orbit magnetic field. The A and B_0 for three samples of different thickness, i.e., S1 (1500 nm), S2 (286 nm), and S3 (348 nm), are summarized in Figure 4c and d, respectively, with the full CD spectra of S2 and S3 shown in Figure S4. Clearly, both A and B_0 depend on the wavelength and the thickness of sample. It has been reported that the frequency-dependent refractive index corresponding to RCP and LCP lights can be expressed as $n^{\pm}(\omega) \approx n(\omega) \pm \frac{dn}{d\omega}\frac{eH}{2mc}$, where ω (c) is the angular frequency (velocity) of light, m is the electron mass, and $n(\omega)$ is the refractive index of the material in the absence of the magnetic field H.[35] Thus, the ΔE, which is proportional to the refractive index difference (Δn), can be

https://doi.org/10.1021/acs.nanolett.4c05724
Nano Lett. 2025, 25, 2709−2715

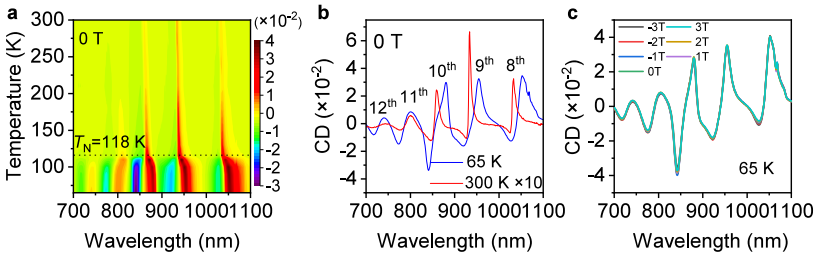

Figure 5. Temperature dependence of cavity-enhanced CD spectra of $FePS_3$. (a) Intensity contour plot of temperature-dependent CD spectra at 0 T. (b) Comparison of CD spectra for $FePS_3$ at 65 and 300 K. The one at 300 K is multiplied by 10. Different CD resonances are marked with their order number (p). (c) Magnetic field-dependent CD spectra of $FePS_3$ at 65 K.

rewritten as $\Delta E \propto \frac{dn}{d\omega}\frac{e}{mc}H$. Therefore, the slope ($A$) of the energy splitting-magnetic field curve is proportional to $\frac{dn}{d\omega}$. According to the measured dispersion curve of the refractive index (n) for $FePS_3$ (Figure 1d), n varies slightly at short wavelengths, which explains the small values of A in the short wavelength regime (Figure 4c). Under the same nominal external magnetic field, the effective magnetic field (B_{eff}) experienced by a thin sample is greater than that by a thick sample, causing a more significant ΔE in the thin sample. Hence, the thin samples (S2 and S3) have relatively larger A values compared to the thickest sample S1, as shown in Figure 4c. However, note that the A we gave here is the nominal slope due to the difference in the effective magnetic field (B_{eff}) among samples of different thicknesses, and the actual slope is independent of the external magnetic field. The external magnetic field-dependent ΔE at different cavity mode resonances carries information about the internal electronic states, which is helpful for further understanding the energy band information on $FePS_3$. The more pronounced ΔE changes with the magnetic field, the larger the magnetic moment of the electron. Regarding B_0, as shown in Figure 4d, the magnitude of B_0 increases with thickness. The increase in B_0 might be because as the $FePS_3$ gets thicker, the degree of inversion symmetry breaking between $FePS_3$ and substrate increases. When the thickness is fixed, for thin samples (S2 and S3), the difference in B_0 between different wavelengths is small, while for thick samples (S1, 1500 nm), the magnitude of B_0 varies greatly with wavelength ranging from about −0.27 T to −0.14 T. Our results suggest that the cavity-enhanced CD technique is an effective probe to detect the broken time-reversal symmetry, inversion asymmetry-induced interfacial spin-orbit magnetic field, and hidden interface state.

To explore the relationships between the nonzero CD at 0 T and different magnetic states of $FePS_3$, we conducted temperature-dependent CD spectra measurements at 0 T. The intensity contour plot of the temperature-dependent CD is displayed in Figure 5a, which shows that the CD magnitude is very weak in the PM state ($T > T_N$), while the CD value increases dramatically below the magnetic phase transition temperature ($T_N \approx 118$ K), reaching a magnitude comparable to that of the CD at −3 T for the PM $FePS_3$. Below T_N, the AFM $FePS_3$, which lacks net magnetization, retains the monoclinic structure. As shown in Figure 1b, the combined centrosymmetric structure and zigzag AFM ordering preserve the inversion symmetry within $FePS_3$ itself, which would prohibit the NCD. However, similar to the case of PM $FePS_3$, the broken inversion symmetry at the interface can induce a finite NCD at 0 T. Besides the structural inversion asymmetry, the spin inversion asymmetry between the zigzag AFM $FePS_3$ and the nonmagnetic substrate also significantly contributes to the larger CD below T_N. Meanwhile, the increased asymmetry in both spin and structure at the interface would also lead to more pronounced B_0 observed in the AFM phase. Before and after the magnetic phase transition, in addition to the obvious difference in CD magnitude, the peak position and line width of the CD also vary, as shown in Figure 5b, which results from the change in the dielectric tensor below and above T_N. To investigate the applied magnetic field response of CD in the AFM state, we measured the CD spectra of the S1 flake (1500 nm) under different external magnetic fields at 65 K, as shown in Figure 5c. For the AFM $FePS_3$, the CD and, thus, the ΔE is almost independent of the external magnetic field below 3 T, in contrast to the linear external magnetic field dependence of ΔE in the PM phase. Since the critical spin-flop field for $FePS_3$ is 35 T,[36] an out-of-plane magnetic field of 3 T is insufficient to rotate the spins. Therefore, the spins in $FePS_3$ remain in the zigzag AFM order, and the CD, which couples to the combined spin and structural inversion asymmetry, would not shift as a function of the external magnetic field below 3 T. Our results demonstrate that constructing an asymmetry interface enables CD to be an effective mean for investigating the magnetic properties of fully compensated collinear AFM materials, including tracking the magnetic phase transition temperature and the spin-flop field.

In conclusion, we demonstrated that cavity-enhanced CD spectroscopy is an effective tool for probing the magnetic order, time-reversal symmetry breaking, and interfacial asymmetries in $FePS_3$. We showed that the external magnetic field induces MCD in the PM state due to the broken time-reversal symmetry, which can be significantly enhanced through the interference effect. By introducing an asymmetric $FePS_3$/substrate interface, we induced a weak but detectable CD signal and an interfacial spin-orbit magnetic field (B_0). It is important to note that this interface effect is particularly crucial in the context of $FePS_3$, an AFM material that does not have net magnetization and where such interfacial symmetry breaking is necessary to observe CD responses. In the AFM state, the CD is strongly coupled with the intrinsic zigzag AFM spin alignment, providing a straightforward way to measure the magnetic phase transition temperature and the spin-flop field, overcoming the challenges of detecting antiferromagnetism due to the lack of net magnetization in fully compensated antiferromagnets. Our work establishes cavity-enhanced CD as a highly sensitive method for detecting broken symmetries in AFM materials and opens the door to using this technique in the study of hidden spin polarizations and interfaces. Furthermore, the ability to tune the CD signal spectrally and in magnitude through external stimuli, such as magnetic fields,

https://doi.org/10.1021/acs.nanolett.4c05724
Nano Lett. 2025, 25, 2709−2715

temperature, and strain, highlights the potential of this approach in developing advanced nanophotonic devices, particularly for circular dichroism-based optical components.

■ ASSOCIATED CONTENT

Supporting Information

The Supporting Information is available free of charge at https://pubs.acs.org/doi/10.1021/acs.nanolett.4c05724.

Cavity-enhanced effect on optical activity and magneto-optical effect, sample preparation, reflectance CD measurements, reflectance and CD simulations, relationship between CD and refractive index difference between LCP and RCP lights, distributed Bragg reflector (DBR) substrate-enhanced CD of thin $FePS_3$, CD spectra of S1 sample at +0 T and −0 T, and full magnetic field-dependent CD spectra of $FePS_3$ (samples S2 and S3) (PDF)

■ AUTHOR INFORMATION

Corresponding Authors

Jun Zhang − *State Key Laboratory of Semiconductor Physics and Chip Technologies, Institute of Semiconductors, Chinese Academy of Sciences, Beijing 100083, China; College of Materials Science and Opto-Electronic Technology, University of Chinese Academy of Sciences, Beijing 100049, China;* orcid.org/0000-0002-9831-6796; Email: zhangjwill@semi.ac.cn

Chao Shen − *State Key Laboratory of Semiconductor Physics and Chip Technologies, Institute of Semiconductors, Chinese Academy of Sciences, Beijing 100083, China; College of Materials Science and Opto-Electronic Technology, University of Chinese Academy of Sciences, Beijing 100049, China;* orcid.org/0000-0002-3664-4874; Email: shenchao@semi.ac.cn

Authors

Shuliang Ren − *State Key Laboratory of Semiconductor Physics and Chip Technologies, Institute of Semiconductors, Chinese Academy of Sciences, Beijing 100083, China; College of Materials Science and Opto-Electronic Technology, University of Chinese Academy of Sciences, Beijing 100049, China;* orcid.org/0000-0001-7708-9398

Simin Pang − *State Key Laboratory of Semiconductor Physics and Chip Technologies, Institute of Semiconductors, Chinese Academy of Sciences, Beijing 100083, China; College of Materials Science and Opto-Electronic Technology, University of Chinese Academy of Sciences, Beijing 100049, China*

Shan Guan − *State Key Laboratory of Semiconductor Physics and Chip Technologies, Institute of Semiconductors, Chinese Academy of Sciences, Beijing 100083, China; College of Materials Science and Opto-Electronic Technology, University of Chinese Academy of Sciences, Beijing 100049, China*

Yu-Jia Sun − *State Key Laboratory of Semiconductor Physics and Chip Technologies, Institute of Semiconductors, Chinese Academy of Sciences, Beijing 100083, China; College of Materials Science and Opto-Electronic Technology, University of Chinese Academy of Sciences, Beijing 100049, China*

Tian-Yu Zhang − *State Key Laboratory of Semiconductor Physics and Chip Technologies, Institute of Semiconductors, Chinese Academy of Sciences, Beijing 100083, China; College of Materials Science and Opto-Electronic Technology, University of Chinese Academy of Sciences, Beijing 100049, China*

Nai Jiang − *State Key Laboratory of Semiconductor Physics and Chip Technologies, Institute of Semiconductors, Chinese Academy of Sciences, Beijing 100083, China; College of Materials Science and Opto-Electronic Technology, University of Chinese Academy of Sciences, Beijing 100049, China*

Jiaqi Guo − *State Key Laboratory of Semiconductor Physics and Chip Technologies, Institute of Semiconductors, Chinese Academy of Sciences, Beijing 100083, China; College of Materials Science and Opto-Electronic Technology, University of Chinese Academy of Sciences, Beijing 100049, China;* orcid.org/0000-0001-5103-345X

Houzhi Zheng − *State Key Laboratory of Semiconductor Physics and Chip Technologies, Institute of Semiconductors, Chinese Academy of Sciences, Beijing 100083, China; College of Materials Science and Opto-Electronic Technology, University of Chinese Academy of Sciences, Beijing 100049, China*

Jun-Wei Luo − *State Key Laboratory of Semiconductor Physics and Chip Technologies, Institute of Semiconductors, Chinese Academy of Sciences, Beijing 100083, China; College of Materials Science and Opto-Electronic Technology, University of Chinese Academy of Sciences, Beijing 100049, China;* orcid.org/0000-0002-1147-8267

Ping-Heng Tan − *State Key Laboratory of Semiconductor Physics and Chip Technologies, Institute of Semiconductors, Chinese Academy of Sciences, Beijing 100083, China; College of Materials Science and Opto-Electronic Technology, University of Chinese Academy of Sciences, Beijing 100049, China;* orcid.org/0000-0001-6575-1516

Complete contact information is available at: https://pubs.acs.org/10.1021/acs.nanolett.4c05724

Author Contributions

J.Z. conceived the project. C.S. and J.Z. designed the experiments. S.R., S.P., and N.J. conducted experiments. T.-Y.Z. and S.R. conducted the simulations of reflectance and CD spectra. S.G. and J.-W.L. analyzed the interfacial spin-orbit magnetic field. S.R., S.P., and J.Z. analyzed the data and wrote the manuscript. All the authors discussed the results and revised the paper.

Author Contributions

†These authors contributed equally (S.R. and S.P.).

Notes

A preprint of this manuscript was posted in arXiv with DOI link 10.48550/arXiv.2411.08667.

The authors declare no competing financial interest.

■ ACKNOWLEDGMENTS

J.Z. acknowledges the funding support from the National Key R&D Program (2024YFA1408203), CAS Project for Young Scientists in Basic Research (YSBR-120), Chinese Academy of Sciences - the Scientific and Technological Research Council of TÜRKİYE Joint Research Projects (172111KYSB20210004). C.S. acknowledges the support from the Youth Innovation Promotion Association, Chinese Academy of Sciences (2019114).

REFERENCES

(1) Sun, Z. Y.; Yi, Y. F.; Song, T. C.; Clark, G.; Huang, B.; Shan, Y. W.; Wu, S.; Huang, D.; Gao, C. L.; Chen, Z. H.; et al. Giant nonreciprocal second-harmonic generation from antiferromagnetic bilayer CrI_3. *Nature* **2019**, *572*, 497−501.

(2) McCreary, A.; Mai, T. T.; Utermohlen, F. G.; Simpson, J. R.; Garrity, K. F.; Feng, X. Z.; Shcherbakov, D.; Zhu, Y. L.; Hu, J.; Weber, D.; et al. Distinct magneto-Raman signatures of spin-flip phase transitions in CrI_3. *Nature Commun.* **2020**, *11*, 3879.

(3) Lee, K.; Dismukes, A. H.; Telford, E. J.; Wiscons, R. A.; Wang, J.; Xu, X. D.; Nuckolls, C.; Dean, C. R.; Roy, X.; Zhu, X. Y. Magnetic Order and Symmetry in the 2D Semiconductor CrSBr. *Nano Lett.* **2021**, *21*, 3511−3517.

(4) Gong, C.; Zhang, X. Two-dimensional magnetic crystals and emergent heterostructure devices. *Science* **2019**, *363*, eaav4450.

(5) Xing, S. C.; Zhou, J.; Zhang, X. G.; Elliott, S.; Sun, Z. M. Theory, properties and engineering of 2D magnetic materials. *Prog. Mater. Sci.* **2023**, *132*, 101036.

(6) Guo, Y. L.; Wang, B.; Zhang, X. W.; Yuan, S. J.; Ma, L.; Wang, J. L. Magnetic two-dimensional layered crystals meet with ferromagnetic semiconductors. *InfoMat* **2020**, *2*, 639−655.

(7) Kurebayashi, H.; Garcia, J. H.; Khan, S.; Sinova, J.; Roche, S. Magnetism, symmetry and spin transport in van der Waals layered systems. *Nat. Rev. Phys.* **2022**, *4*, 150−166.

(8) Stephens, P. J. Magnetic circular-dichroism. *Annu. Rev. Phys. Chem.* **1974**, *25*, 201−232.

(9) Woody, R. W. Circular-Dichroism. *Biochemical Spectroscopy*; Academic Press, 1995; pp 34−71.

(10) Govorov, A. O.; Fan, Z. Y.; Hernandez, P.; Slocik, J. M.; Naik, R. R. Theory of circular dichroism of nanomaterials comprising chiral molecules and nanocrystals: plasmon enhancement, dipole interactions, and dielectric effects. *Nano Lett.* **2010**, *10*, 1374−1382.

(11) Han, B.; Gao, X. Q.; Lv, J. W.; Tang, Z. Y. Magnetic circular dichroism in nanomaterials: new opportunity in understanding and modulation of excitonic and plasmonic resonances. *Adv. Mater.* **2020**, *32*, 1801491.

(12) Mason, W. R. Introduction. *A Practical Guide to Magnetic Circular Dichroism Spectroscopy*; John Wiley & Sons, Inc., 2007; pp 1−3.

(13) Barron, L. D. *Molecular Light Scattering and Optical Activity*; Cambridge University Press, 2009.

(14) Mak, K. F.; Shan, J.; Ralph, D. C. Probing and controlling magnetic states in 2D layered magnetic materials. *Nat. Rev. Phys.* **2019**, *1*, 646−661.

(15) Jungwirth, T.; Marti, X.; Wadley, P.; Wunderlich, J. Antiferromagnetic spintronics. *Nat. Nanotechnol.* **2016**, *11*, 231−241.

(16) Duine, R. A.; Lee, K. J.; Parkin, S. S. P.; Stiles, M. D. Synthetic antiferromagnetic spintronics. *Nat. Phys.* **2018**, *14*, 217−219.

(17) Nemec, P.; Fiebig, M.; Kampfrath, T.; Kimel, A. V. Antiferromagnetic opto-spintronics. *Nat. Phys.* **2018**, *14*, 229−241.

(18) Lee, J. U.; Lee, S.; Ryoo, J. H.; Kang, S.; Kim, T. Y.; Kim, P.; Park, C. H.; Park, J. G.; Cheong, H. Ising-type magnetic ordering in atomically thin $FePS_3$. *Nano Lett.* **2016**, *16*, 7433−7438.

(19) Lançon, D.; Walker, H. C.; Ressouche, E.; Ouladdiaf, B.; Rule, K. C.; McIntyre, G. J.; Hicks, T. J.; Ronnow, H. M.; Wildes, A. R. Magnetic structure and magnon dynamics of the quasi-two-dimensional antiferromagnet $FePS_3$. *Phys. Rev. B* **2016**, *94*, 214407.

(20) Lee, Y.; Son, S.; Kim, C.; Kang, S.; Shen, J. Y.; Kenzelmann, M.; Delley, B.; Savchenko, T.; Parchenko, S.; Na, W.; et al. Giant magnetic anisotropy in the atomically thin van der Waals antiferromagnet $FePS_3$. *Adv. Electron. Mater.* **2023**, *9*, 2200650.

(21) Zhang, H. Q.; Ni, Z. L.; Stevens, C. E.; Bai, A. F.; Peiris, F.; Hendrickson, J. R.; Wu, L.; Jariwala, D. Cavity-enhanced linear dichroism in a van der Waals antiferromagnet. *Nat. Photonics* **2022**, *16*, 311−317.

(22) Ni, Z. L.; Huang, N.; Haglund, A. V.; Mandrus, D. G.; Wu, L. Observation of giant surface second-harmonic generation coupled to nematic orders in the van der Waals antiferromagnet $FePS_3$. *Nano Lett.* **2022**, *22*, 3283−3288.

(23) Zhang, X. X.; Jiang, S. W.; Lee, J.; Lee, C. G.; Mak, K. F.; Shan, J. Spin Dynamics slowdown near the antiferromagnetic critical point in atomically thin $FePS_3$. *Nano Lett.* **2021**, *21*, 5045−5052.

(24) Liu, S.; del Aguila, A. G.; Bhowmick, D.; Gan, C. K.; Do, T. T. H.; Prosnikov, M. A.; Sedmidubsky, D.; Sofer, Z.; Christianen, P. C. M.; Sengupta, P.; et al. Direct observation of magnon-phonon strong coupling in two-dimensional antiferromagnet at high magnetic fields. *Phys. Rev. Lett.* **2021**, *127*, 097401.

(25) Du, K. Z.; Wang, X. Z.; Liu, Y.; Hu, P.; Utama, M. I. B.; Gan, C. K.; Xiong, Q. H.; Kloc, C. Weak van der Waals stacking, wide-range band gap, and Raman study on ultrathin layers of metal phosphorus trichalcogenides. *ACS Nano* **2016**, *10*, 1738−1743.

(26) Jernberg, P.; Bjarman, S.; Wappling, R. $FePS_3$: A first-order phase transition in a "2D" Ising antiferromagnet. *J. Magn. Magn. Mater.* **1984**, *46*, 178−190.

(27) Zhou, F. R.; Liu, H. H.; Zajac, M.; Hwangbo, K.; Jiang, Q. N.; Chu, J. H.; Xu, X. D.; Arslan, I.; Gage, T. E.; Wen, H. D. Ultrafast nanoimaging of spin-mediated shear waves in an acoustic cavity. *Nano Lett.* **2023**, *23*, 10213−10220.

(28) Feng, W. X.; Guo, G. Y.; Zhou, J.; Yao, Y. G.; Niu, Q. Large magneto-optical Kerr effect in noncollinear antiferromagnets Mn_3X (X = Rh, Ir, Pt). *Phys. Rev. B* **2015**, *92*, 144426.

(29) Kats, M. A.; Blanchard, R.; Genevet, P.; Capasso, F. Nanometre optical coatings based on strong interference effects in highly absorbing media. *Nat. Mater.* **2013**, *12*, 20−24.

(30) Wu, Y. J.; Shen, C.; Tan, Q. H.; Shi, J.; Liu, X. F.; Wu, Z. H.; Zhang, J.; Tan, P. H.; Zheng, H. Z. Valley Zeeman splitting of monolayer MoS_2 probed by low-field magnetic circular dichroism spectroscopy at room temperature. *Appl. Phys. Lett.* **2018**, *112*, 153105.

(31) Mason, W. R. Theoretical Framework: Definition of MCD Terms. *A Practical Guide to Magnetic Circular Dichroism Spectroscopy*; John Wiley & Sons, Inc., 2007; pp 14−35.

(32) Sugano, S.; Kojima, N. *Magneto-Optics*; Springer Science & Business Media, 2013.

(33) Chen, L.; Gmitra, M.; Vogel, M.; Islinger, R.; Kronseder, M.; Schuh, D.; Bougeard, D.; Fabian, J.; Weiss, D.; Back, C. H. Electric-field control of interfacial spin-orbit fields. *Nat. Electron.* **2018**, *1*, 350−355.

(34) Soumyanarayanan, A.; Reyren, N.; Fert, A.; Panagopoulos, C. Emergent phenomena induced by spin-orbit coupling at surfaces and interfaces. *Nature* **2016**, *539*, 509−517.

(35) Ruan, Y. L.; Jarvis, R. A.; Rode, A. V.; Madden, S.; Luther-Davies, B. Wavelength dispersion of Verdet constants in chalcogenide glasses for magneto-optical waveguide devices. *Opt. Commun.* **2005**, *252*, 39−45.

(36) Wildes, A. R.; Lançon, D.; Chan, M. K.; Weickert, F.; Harrison, N.; Simonet, V.; Zhitomirsky, M. E.; Gvozdikova, M. V.; Ziman, T.; Ronnow, H. M. High field magnetization of $FePS_3$. *Phys. Rev. B* **2020**, *101*, 024415.

https://doi.org/10.1021/acs.nanolett.4c05724
Nano Lett. 2025, 25, 2709−2715